

**Paleoclimate pattern effects strongly constrain modern
climate sensitivity and 21st-century warming**

**V. T. Cooper^{1*}, K. C. Armour^{1,2}, G. J. Hakim¹, J. E. Tierney³, N. J. Burls⁴,
C. Proistosescu⁵, T. Andrews^{6,7}, W. Dong^{8,9}, M. T. Dvorak², R. Feng¹⁰, M. B.
Osman¹¹, Y. Dong¹²**

¹Department of Atmospheric and Climate Science, University of Washington, Seattle, WA, USA

²School of Oceanography, University of Washington, Seattle, WA, USA

³Department of Geosciences, University of Arizona, Tucson, AZ, USA

⁴Department of Atmospheric, Oceanic and Earth Sciences, George Mason University, Fairfax, VA, USA

⁵Department of Climate, Meteorology, and Atmospheric Sciences, University of Illinois at

Urbana-Champaign, Champaign, IL, USA

⁶Met Office Hadley Centre, Exeter, UK

⁷School of Earth and Environment, University of Leeds, Leeds, UK

⁸Cooperative Programs for the Advancement of Earth System Science, University Corporation for

Atmospheric Research, Boulder, CO, USA

⁹NOAA/Geophysical Fluid Dynamics Laboratory, Princeton, NJ, USA

¹⁰Department of Geosciences, University of Connecticut, Storrs, CT, USA

¹¹Department of Geography, The University of Cambridge, Cambridge, UK

¹²Department of Atmospheric and Oceanic Sciences, University of California Los Angeles, Los Angeles,

CA, USA

Corresponding author: *Vincent T. Cooper, vcooper@uw.edu

21 **Abstract**

22 Paleoclimates provide examples of past climate change that inform estimates of mod-
 23 ern warming from greenhouse-gas emissions, known as Earth's climate sensitivity. How-
 24 ever, differences between past and present climate change must be accounted for when
 25 inferring climate sensitivity from paleoclimate evidence [1–3]. The Pliocene (5.3–2.6 Ma),
 26 a warm epoch with atmospheric CO₂ concentrations similar to today, is a potential ana-
 27 log for modern warming [4]. Recent reconstructions indicate the Pliocene was 1°C warmer
 28 than previously thought [5, 6], implying higher climate sensitivity [5], supported by re-
 29 constructions of more global cooling from reduced CO₂ at the Last Glacial Maximum
 30 (LGM; 19–23 thousand years ago) [7–9]. However, these same reconstructions indicate
 31 large-scale patterns of paleoclimate temperature change differ strongly from modern pro-
 32 jections. Climate feedbacks and sensitivity depend on temperature patterns [e.g., 10–
 33 14], and such “pattern effects” must be accounted for when using paleoclimates to con-
 34 strain modern climate sensitivity [3]. Here we combine data-assimilation reconstructions
 35 with atmosphere models to show Earth's climate is more sensitive to Pliocene forcing
 36 than modern CO₂ forcing. Pliocene ice sheets, topography, and vegetation alter patterns
 37 of ocean warming and excite destabilizing cloud feedbacks, and LGM feedbacks are sim-
 38 ilarly amplified by the North American ice sheet. Accounting for paleoclimate pattern
 39 effects produces a best estimate (median) for modern climate sensitivity of 2.8°C, 66%
 40 range 2.4 – 3.4°C (90% CI: 2.1 – 4.0°C), substantially reducing uncertainty and nar-
 41 rowing projections of 21st-century warming.

42 **Main Text**

43 The paleoclimate record constitutes a series of natural experiments with fundamen-
 44 tal insights into Earth's climate sensitivity. Using paleoclimate evidence to constrain the
 45 modern sensitivity to rising greenhouse-gas concentrations requires accounting for dif-
 46 ferences in both climate forcings and feedbacks between the past and modern climates
 47 [1–3]. A key driver of such feedback differences across past climates is variation in the
 48 spatial pattern of sea-surface temperature, i.e., “paleoclimate pattern effects” [3]. Pat-
 49 tern effects are variations in climate sensitivity and feedbacks that depend on spatial pat-
 50 terns of temperature change [e.g., 10–14], and they arise in paleoclimate contexts when
 51 non-CO₂ forcings (such as ice sheets, topography, and vegetation) affect large-scale tem-
 52 perature patterns. Paleoclimate pattern effects can have major impacts on estimates of
 53 modern climate sensitivity if non-CO₂ forcings strongly influence the temperature pat-
 54 tern, thereby producing climate feedbacks that differ from those that govern modern warm-
 55 ing from greenhouse-gas forcing [3].

56 The Pliocene (5.3–2.6 Ma) is the closest analog to near-term warming [4]. Its mid-
 57 Piacenzian warm period (c. 3.3–3.0 Ma), hereafter “Pliocene,” is the most recent epoch
 58 with atmospheric concentrations of CO₂ (near 400 ppm) that are similar to present day
 59 [15]. The magnitude of Pliocene warming thus provides an important constraint on the
 60 equilibrium climate sensitivity (ECS) of the modern climate, which is the equilibrium
 61 response of global-mean near-surface air temperature to a doubling of atmospheric CO₂
 62 from preindustrial levels [2, 16]. Previous assessments of paleoclimate proxies report ap-
 63 proximately 3°C of global-mean Pliocene warming and an upper bound of 4°C relative
 64 to preindustrial conditions [2, 16]. However, recent reconstructions find a much warmer
 65 Pliocene, with central estimates of 4°C [5, 6]. This Pliocene warming suggests a much

higher ECS of 4.8°C [5], implying increased likelihood of realizing the worst-case projections of 21st-century warming. But these globally resolved reconstructions tell us more than global means—they capture the spatial pattern of Pliocene warming, and this spatial information is essential to constraining modern ECS.

To infer modern ECS from Pliocene evidence, we must consider differences in both forcing and feedbacks between the Pliocene and present climate. The Pliocene has both elevated greenhouse-gas (GHG) forcings [15, 17] as well as additional forcing from (i) reduced ice sheets over West Antarctica and Greenland, (ii) increased vegetation, especially over northern high latitudes, and (iii) changes in land-sea distribution [1, 2, 18, 19]. Previous work found that the Pliocene’s global-mean warming is mostly attributable to CO₂ [20–22]. However, modeling studies show that the non-CO₂ forcings drive distinct climate responses especially at regional scales [20, 22–27], and Pliocene temperature patterns may differ substantially from those in response to modern CO₂ forcing [23], thereby producing different climate feedbacks. Accounting for such pattern effects in the Last Glacial Maximum (LGM), a cold period 19–23 ka, led to stronger constraints on modern ECS [3]. The key question here is, would accounting for Pliocene pattern effects also strengthen constraints on modern ECS?

We quantify Pliocene pattern effects by synthesizing proxy data with climate models, and we use these results to revise estimates of modern ECS and 21st-century warming. Spatially complete reconstructions of the Pliocene [5, 6] from paleoclimate data assimilation [7, 8, 28] are used in numerical experiments with five atmospheric general circulation models (AGCMs) to quantify relationships between temperature patterns and climate feedbacks [e.g., 3, 11]. We analyze differences between feedbacks in the Pliocene compared to modern warming from CO₂. We then combine our Pliocene results with an investigation of the LGM [3], and we quantify the impacts of the feedback differences on estimates of modern ECS and projections 21st-century warming.

92 Paleoclimate Pattern Effects and Modern ECS

93 Modern ECS, climate feedbacks, and paleoclimate pattern effects are related through
94 the global-mean energy balance,

$$95 \quad \Delta N = \Delta F + \lambda \Delta T, \quad (1)$$

96 where ΔN is the change in top-of-atmosphere radiative balance; ΔF is the “effective”
97 radiative forcing, i.e., the change in net downward radiative flux after atmospheric ad-
98 justments to imposed perturbations, excluding radiative responses to changing surface
99 temperature [16]; λ is the net climate feedback (negative for stable climates); and ΔT
100 is the change in near-surface air temperature. All values are global means, and differ-
101 ences (Δ) are relative to the preindustrial baseline. When the forcing is a doubling of
102 preindustrial CO₂ concentrations (2xCO₂), and the climate reaches equilibrium ($\Delta N =$
103 0), the resulting ΔT is the modern ECS:

$$104 \quad \text{ECS} = -\Delta F_{2x\text{CO}_2} / \lambda_{2x\text{CO}_2}. \quad (2)$$

105 In this case, $\Delta F_{2x\text{CO}_2}$ is the effective radiative forcing and $\lambda_{2x\text{CO}_2}$ is the net feedback
106 from modern CO₂ doubling. Increasingly negative values of λ indicate more-stable cli-
107 mates and lower ECS.

Paleoclimate pattern effects ($\Delta\lambda$) are quantified as the difference between λ_{2xCO_2} and a paleoclimate feedback, e.g., the Pliocene feedback (λ_{Plio}), due to differences in the spatial patterns of warming:

$$\Delta\lambda = \lambda_{2xCO_2} - \lambda_{Plio}. \quad (3)$$

$\Delta\lambda$ also can vary with global-mean temperature [e.g., 2, 3, 29]. Temperature dependence can be omitted for the Pliocene due to similar levels of warming from Pliocene and $2xCO_2$ forcings [2] and is relatively small for LGM levels of cooling [3, 30].

Modern ECS and λ_{2xCO_2} can be constrained by estimating λ_{Plio} and $\Delta\lambda$, then combining Equations 2 and 3:

$$ECS = -\Delta F_{2xCO_2}/(\lambda_{Plio} + \Delta\lambda). \quad (4)$$

$\Delta\lambda$ depends on spatial patterns of Pliocene temperature anomalies, for which we use state-of-the-art reconstructions from data assimilation [5, 6] as boundary conditions for experiments using five AGCMs, as described in the following section.

Pliocene Pattern Effects Constrained by Data Assimilation

SST Patterns from Data Assimilation

In Fig. 1, we compare the projected sea-surface temperature (SST) anomalies from modern $2xCO_2$, based on the multi-model mean of quasi-equilibrium simulations in LongRunMIP [31], with the various Pliocene reconstructions from “plioDA” [5] and ref. [6] that we use to quantify Pliocene pattern effects. The Pliocene patterns include the best estimates from plioDA [5] and ref. [6], as well as alternate plioDA reconstructions that test structural uncertainty and endmembers of the plioDA ensemble (Fig. 1; Fig. S1–S4) (Methods). The reconstructions use paleoclimate data assimilation [7, 8, 28], which optimally combines dynamical constraints from model “priors” with proxy data. Data assimilation results depend on specific aspects of the methods, model priors [32], and observations.

To address reconstruction uncertainty, we analyze pattern effects across a wide range of possible Pliocene temperature patterns that use different assimilation methods, model priors, and subsets of proxy data. Focusing on sensitivity to the model prior, the “PlioMIP2 Prior” version of plioDA uses 14 PlioMIP2 simulations [33] to inform its prior. The “Perturbed Cloud Prior” uses 21 simulations that are designed to capture Pliocene temperature gradients by substantially altering models’ cloud physics, while non-GHG forcings are unchanged from preindustrial conditions [34–36]. Focusing on sensitivity to the proxy network, the “PlioVar Data” version restricts data to the KM5c interglacial [37], and we also test endmembers of the plioDA ensemble (Fig. S4) (Methods). Ref. [6] and plioDA [5] have partially overlapping proxy networks, model priors (both best estimates include simulations from PlioMIP2), and assimilation methods (ensemble Kalman filter); however, there are substantial differences between the two reconstruction efforts in terms of the proxies included, model priors, and methods (e.g., forward modeling of proxies in plioDA) that lead to differences in their results [5] (Fig. 1b,f).

Despite the substantial uncertainty in the details of the Pliocene SST patterns shown in Fig. 1, the reconstructions all have two common features that distinguish the Pliocene from the modern response to $2xCO_2$: the Pliocene has amplified SST warming in the Southern Ocean and in the North Atlantic (Fig. 1; Fig. S1). It is also clear that the spatial

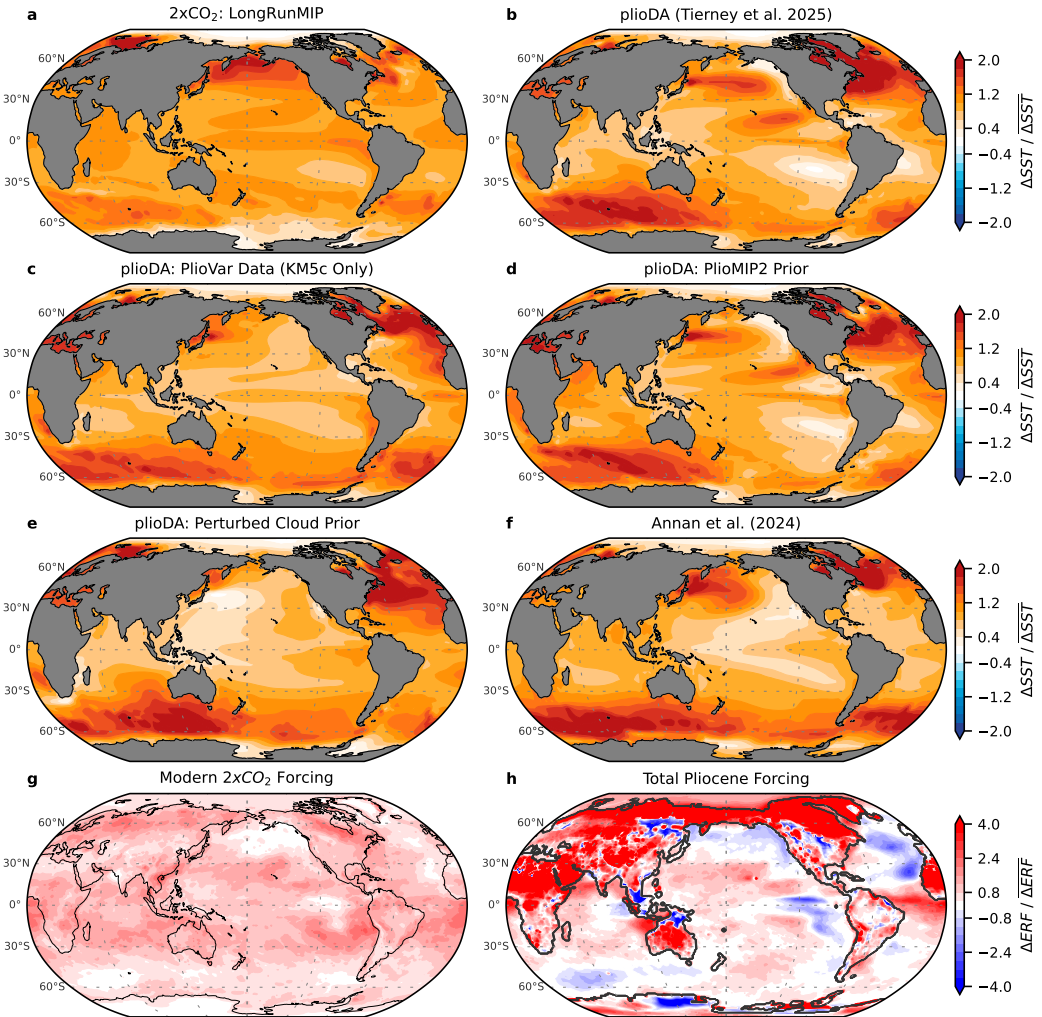


Figure 1. Patterns of sea-surface temperature (SST) anomalies and effective radiative forcing (ERF). (A) Multi-model mean of modern SST response to 2CO_2 in quasi-equilibrium simulations from LongRunMIP [31]. (B–F) Data-assimilation reconstructions from: (B) plioDA best estimate [5]; alternate plioDA using (C) only the PlioVar proxy data representing the KM5c interglacial, (D) only the PlioMIP2 prior, or (E) only the perturbed-cloud prior; and (F) best estimate from ref. [6]. ERF from (G) modern 2CO_2 and (H) Pliocene total forcing, including greenhouse gases, reduced Greenland and Antarctic ice sheets, sea level, and vegetation [23]. All panels show annual-mean anomalies, and local values are divided by global means. Pliocene SSTs are infilled to modern coastlines.

151 pattern of *forcing* during the Pliocene (Fig. 1h) differs substantially from the relatively
 152 uniform forcing produced by CO₂ alone (Fig. 1g) because of the Pliocene's non-CO₂ forcings,
 153 such as changes in ice sheets, topography, and vegetation [23]. The connection be-
 154 tween the non-CO₂ Pliocene forcings and the distinct SST patterns they produce has
 155 been illustrated in coupled-model experiments [23], which we return to in the Discus-
 156 sion.

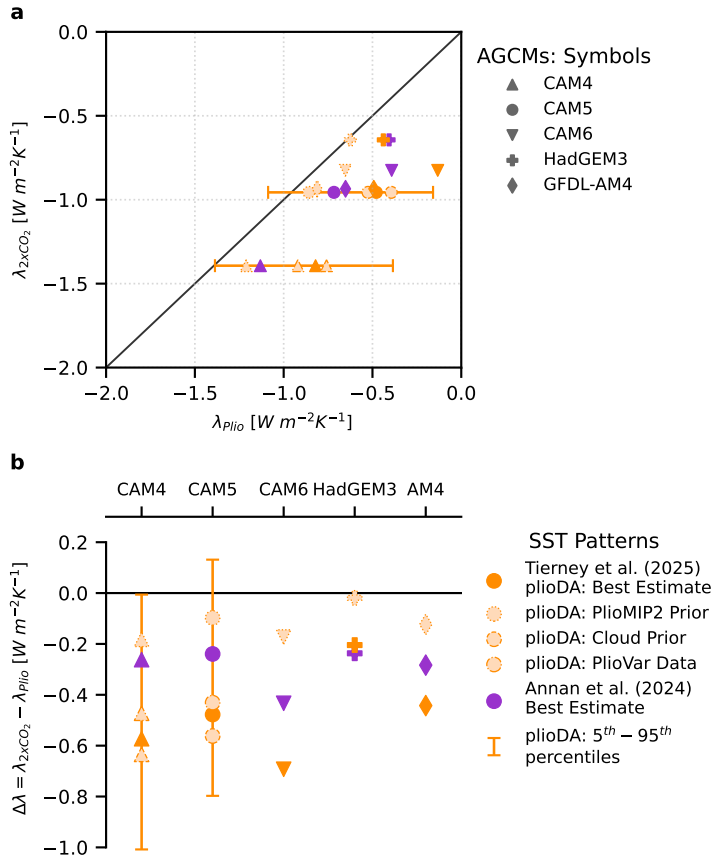


Figure 2. Net climate feedbacks (λ) and Pliocene pattern effect ($\Delta\lambda$). Note that each legend applies to both panels; different atmospheric general circulation models (AGCMs) are denoted by symbols, and different Pliocene warming patterns are denoted by colors and borders. (a) Scatter plot of λ_{2xCO_2} versus λ_{Plio} for each AGCM and Pliocene pattern, with $\lambda_{2xCO_2} = \lambda_{Plio}$ shown as solid line. (b) Pliocene pattern effect, $\Delta\lambda = \lambda_{2xCO_2} - \lambda_{Plio}$, using values in panel a. Error bars for plioDA represent endmembers of the ensemble reconstruction (Methods).

157 Quantifying Feedbacks and Pattern Effects

158 We estimate the net climate feedback, λ , for each warming pattern in Fig. 1 us-
 159 ing AGCM experiments with prescribed SST and sea-ice concentration (SIC) (Methods).
 160 Following ref. [3], we begin with a control experiment using the preindustrial “baseline”
 161 pattern [8]. We repeat the AGCM experiments, changing only the SST and SIC to the
 162 2xCO₂ pattern from LongRunMIP (Fig. 1a) and to each of the Pliocene patterns (Fig.
 163 1b–e; SIC in Fig. S2–S4). We hold the forcings constant across all simulations to iso-
 164 late the radiative response to surface temperatures (Methods). For each experiment, we

165 calculate ΔN and ΔT relative to the preindustrial baseline, and the net feedback is $\lambda = \Delta N/\Delta T$ from Eq. 1 with $\Delta F = 0$.

167 In Fig. 2, we compare λ_{2xCO_2} with λ_{Plio} and quantify Pliocene pattern effects ($\Delta\lambda$).
 168 In all five AGCMs, λ_{Plio} is more positive (destabilizing) than λ_{2xCO_2} , which means that
 169 the climate system is more sensitive to Pliocene forcing than it is to modern $2xCO_2$ forc-
 170 ing. We test whether this result is robust despite uncertainties in atmospheric model physics
 171 and Pliocene reconstructions by running the experiments in CAM4, CAM5, CAM6, GFDL-
 172 AM4, and HadGEM3-GC3.1-LL, and by testing three different Pliocene patterns (Fig
 173 1B,D,F) in all five AGCMs. We test additional Pliocene patterns, including the 5th and
 174 95th percentiles of the plioDA ensemble (Fig. S4), in CAM4 and CAM5 (Methods). De-
 175 spite the uncertainties in Pliocene SST patterns and atmospheric model physics, there
 176 is a clear Pliocene pattern effect with $\Delta\lambda < 0$ (Fig. 2b), albeit with uncertain magni-
 177 tude.

178 In summary, the Pliocene warming pattern excites more positive (destabilizing) cli-
 179 mate feedbacks compared to the $2xCO_2$ warming pattern ($\lambda_{Plio} > \lambda_{2xCO_2}$), i.e., the Pliocene
 180 pattern effect is negative ($\Delta\lambda < 0$). As will be shown below, the negative pattern ef-
 181 fect indicates that positive feedbacks amplified Pliocene warming, but those feedbacks
 182 do not play an equivalent role in the modern climate's response to greenhouse-gas forc-
 183 ing. Accounting for this negative Pliocene pattern effect would lead to lower estimates
 184 of modern ECS and future warming (Eq. 4) [3].

185 Discussion

186 Mechanisms Responsible for Pliocene Pattern Effects

187 To diagnose the mechanisms contributing to more-positive climate feedbacks in the
 188 Pliocene, we first use radiative kernels to assess each component feedback (Methods) [38].
 189 We find that the cloud feedback (λ_{cloud}), namely the shortwave component associated
 190 with low clouds, is the dominant driver of $\lambda_{Plio} > \lambda_{2xCO_2}$ (Fig. S5–S6). The combined
 191 lapse-rate and water-vapor feedbacks make an additional contribution to more-positive
 192 λ_{Plio} (Fig. S5). Next, we inspect the spatial distribution of the Pliocene's more-positive
 193 cloud feedbacks to understand their source.

194 In Fig. 3, we compare the spatial patterns of λ_{cloud} in the Pliocene versus $2xCO_2$.
 195 The most pronounced differences are over the Southern Ocean (Indian sector) and the
 196 North Atlantic. The zonal mean of $\Delta\lambda_{cloud}$ (Fig. 3a) illustrates that the Pliocene's ex-
 197 tratropical cloud feedbacks are responsible for λ_{Plio} being more positive than λ_{2xCO_2} , sup-
 198 ported by extratropical lapse-rate feedbacks (Fig. S9). Comparing Fig. 3's λ_{cloud} with
 199 Fig. 1's SST patterns (zonal mean SST in Fig. S10), we see that the regions with am-
 200 plified Pliocene SST anomalies are approximately collocated with the amplified Pliocene
 201 λ_{cloud} . Consistent with a similar analysis of the Last Glacial Maximum [3], amplified SST
 202 anomalies in the extratropics are responsible for more-positive feedbacks in the Pliocene.
 203 When SST warming is strongly amplified in the extratropics compared to the SST warm-
 204 ing in tropical regions of atmospheric deep convection (e.g., the west Pacific warm pool),
 205 tropospheric stability is decreased and low-cloud cover is reduced, which is a positive feed-
 206 back on the initial warming [13, 39]. Past studies of the Pliocene emphasize the zonal
 207 SST in the tropical Pacific and meridional temperature gradients [5, 21, 40–44], while

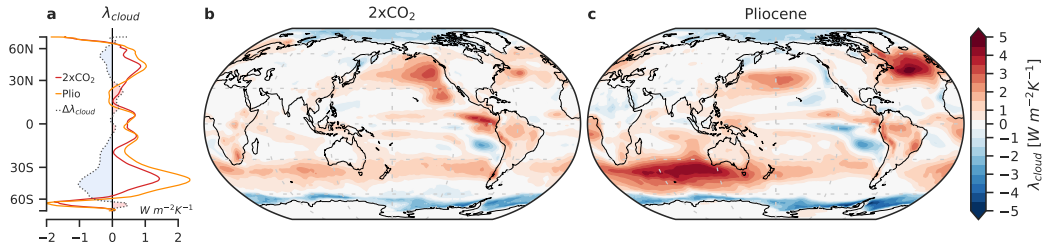


Figure 3. Cloud feedbacks from modern CO₂ forcing versus Pliocene warming.

(a) Zonal means of panels b, c, and their difference, $\Delta\lambda_{\text{cloud}}$; negative values of $\Delta\lambda_{\text{cloud}}$ contribute to the negative Pliocene pattern effect. (b–c) Spatial distributions of cloud feedbacks, $\lambda_{\text{cloud}} = \Delta N_{\text{local}}/\overline{\Delta T}$, where ΔN_{local} is the local anomaly in top-of-atmosphere radiation attributable to cloud feedbacks (estimated with radiative kernels), and $\overline{\Delta T}$ is the global-mean T anomaly. Multi-model mean of (b) λ_{cloud} using the LongRunMIP 2xCO₂ pattern and (c) multi-pattern mean λ_{cloud} from Pliocene patterns in Fig. 1b,d,f (plioDA best estimate [5], alternate plioDA using only the PlioMIP2 prior, and ref. [6] best estimate; these patterns were tested in all atmosphere models). All panels show multi-model means across atmosphere models.

we find that the amplification of warming in the North Atlantic and especially the Southern Ocean are the dominant features that distinguish Pliocene feedbacks from the modern response to 2xCO₂.

The final and essential aspect of the mechanism is that amplified warming in the Southern Ocean and North Atlantic is due to non-CO₂ forcings (ice sheets, vegetation, and topography), as shown in Fig. S11. This attribution has been illustrated by experiments in coupled models that separate the SST response to Pliocene CO₂ versus non-CO₂ forcings [e.g., 20, 22, 23, 33]. Pliocene warming in the North Atlantic is amplified by the closure of ocean gateways (Bering Strait and Canadian Archipelago) through changes in the Atlantic Meridional Overturning Circulation (AMOC) [24], and it is further amplified by reductions in ice sheets [26]. Amplified warming in the Southern Ocean is associated with the reduced Antarctic Ice Sheet and topography through changes in ocean circulation [23, 45]. While amplified warming of the Southern Ocean appears in all reconstructions (Fig. 1), its magnitude is uncertain due to sparse proxy data, and this uncertainty makes a large contribution to our spread in $\Delta\lambda$ (Fig. S8–S10). Compared to coupled models, both the North Atlantic and Southern Ocean SST features are even more pronounced in data-assimilation reconstructions constrained by paleoclimate proxies (Fig. 1) [5, 6]. Thus coupled models are essential for illustrating mechanisms of paleoclimate pattern effects, and incorporating observational constraints through data assimilation is key to producing reliable SST patterns and constraining uncertainty in $\Delta\lambda$.

While our comparison of the Pliocene versus modern 2xCO₂ uses the LongRunMIP pattern [31], we note that there is substantial uncertainty in the projected SST pattern from 2xCO₂. However, the mechanism of Pliocene and LGM pattern effects is based on how non-CO₂ forcings impact paleoclimate temperature patterns, thus we expect conclusions about $\Delta\lambda$ to be relatively insensitive to uncertainty in the SST pattern from CO₂ forcing. Furthermore, ref. [46] finds that the feedback uncertainty from CO₂ patterns is only 10% of the spread across different models, which emphasizes the importance of

235 using multiple AGCMs to quantify uncertainty in $\Delta\lambda$. We also test whether results are
 236 sensitive to the 2xCO₂ pattern and find this uncertainty does not affect the conclusions
 237 (Methods).

238 In summary, non-CO₂ forcings from ice sheets, topography, and vegetation altered
 239 the spatial pattern of ocean warming, in turn producing positive cloud feedbacks in the
 240 extratropics that strongly amplify global warming (Fig. 3). Because of these amplifying
 241 feedbacks, more of the Pliocene warming was caused by non-CO₂ forcings than previously
 242 thought, meaning that less of the warming is attributable to elevated CO₂ alone.
 243 Since these amplifying feedbacks from non-CO₂ forcing do not play a role in the modern
 244 response to 2xCO₂ alone, we now show that accounting for the Pliocene pattern effect
 245 lowers estimates of modern ECS and reduces the likelihood of worst-case projections
 246 for 21st-century warming.

247 Modern Climate Sensitivity and 21st-Century Warming

248 To constrain modern ECS with paleoclimate evidence, we first infer climate feedbacks
 249 during a paleoclimate period from changes in Earth's energy budget, and then we
 250 account for differences relative to the modern response to 2xCO₂ [1–3]. Measures of
 251 climate sensitivity depend on the timescale of interest, and we follow ref. [2], hereafter “SW20,”
 252 in focusing on the 150-year timescale of “effective” climate sensitivity (S), and in treating
 253 slow paleoclimate feedbacks, e.g., ice sheets, as radiative forcings [1].

254 First, we estimate λ_{Plio} by applying Equation 1 to the Pliocene (Methods). We update
 255 ΔT_{Plio} from SW20's values of 3.0 ± 1.0 °C (1σ) to plioDA's result of $\Delta T_{\text{Plio}} =$
 256 4.1 ± 0.6 °C (1σ). We also update the non-GHG (greenhouse gas) effective radiative forcing
 257 to $\Delta F_{\text{NonGHG}} = 1.7 \pm 1.0$ (1σ) W m⁻² [23]. Given that $\Delta F_{\text{GHG}} \approx 2.2$ W m⁻² [2,
 258 23], we have a central estimate of total $\Delta F_{\text{Plio}} = 3.9$ W m⁻² and $\lambda_{\text{Plio}} \approx -1.0$ W m⁻² K⁻¹
 259 (Methods).

260 The novel aspect of the modern ECS constraint in this study is the inclusion of paleoclimate
 261 pattern effects for the Pliocene ($\Delta\lambda$; Eq. 3 and 4) and the synthesis with pattern
 262 effects for the Last Glacial Maximum [3]. We combine uncertainty across SST patterns
 263 and atmospheric models (Fig. 2; Methods), which produces a central estimate for
 264 Pliocene pattern effects of $\Delta\lambda = -0.37 \pm 0.32$ (1σ) W m⁻² K⁻¹. We adapt the Bayesian
 265 framework of SW20 to include Pliocene $\Delta\lambda$, following ref. [3] (Methods).

266 In Fig. 4a, we show the S likelihoods from Pliocene evidence alone. For comparison,
 267 we include the original SW20 results and the likelihood with updated Pliocene global-
 268 mean ΔT and ΔF_{NonGHG} but excluding Pliocene pattern effects. As seen in Fig. 4a, the
 269 updates from the *global-mean* information alone (excluding $\Delta\lambda$) suggest a much higher
 270 ECS [5]. However, the *spatial information* in the Pliocene reconstructions—quantified
 271 as $\Delta\lambda$ —has a larger and opposite impact. Including $\Delta\lambda$ shifts the maximum likelihood
 272 from 3.7°C to 2.7°C and has a pronounced influence on reducing the high tail of the distribution.

273 We now revise the best estimate for modern ECS by combining the Pliocene with
 274 the additional lines of evidence in SW20: the Last Glacial Maximum (LGM), the historical
 275 record (c. 1870–present), and process understanding (Methods) (Fig. 4b). We
 276 first show SW20's results, then we include paleoclimate updates only to global-mean quan-

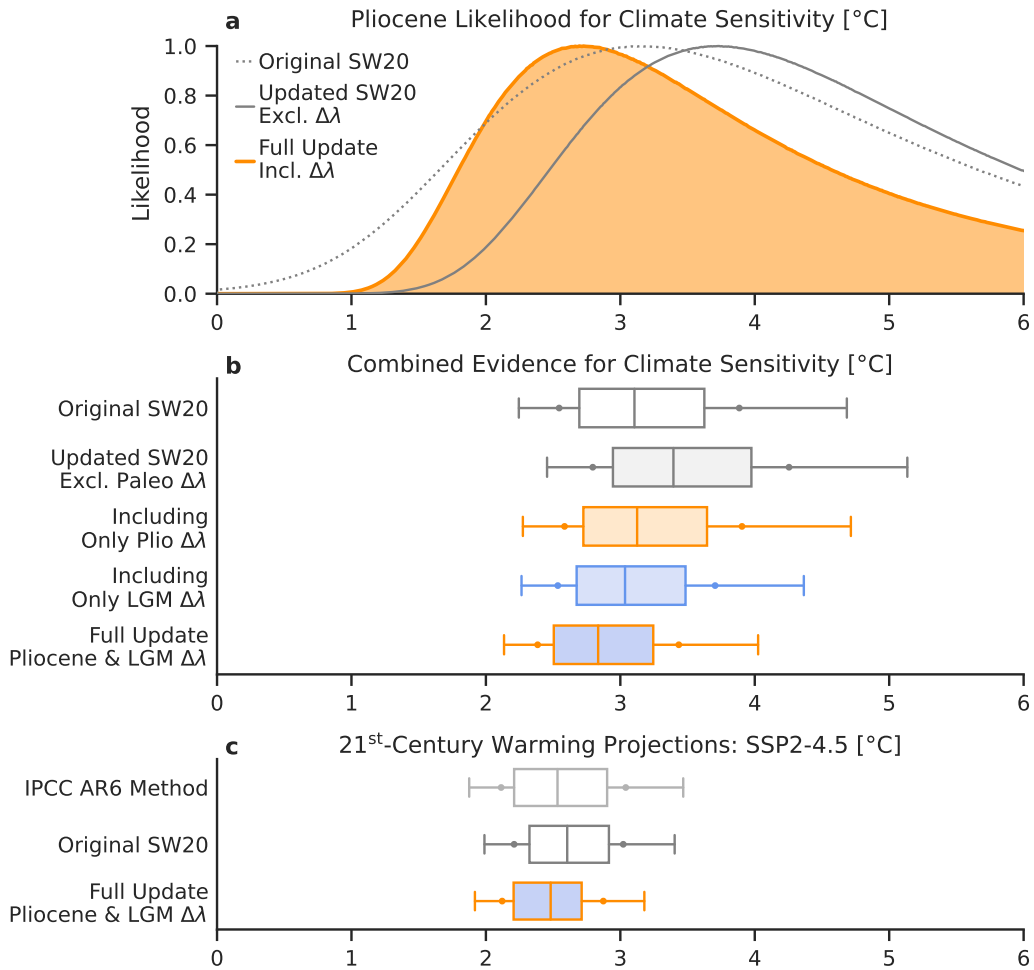


Figure 4. Modern climate sensitivity and 21st-century warming, accounting for paleoclimate pattern effects ($\Delta\lambda$). (a) Pliocene-only likelihoods (dotted) from SW20 [2]; (gray) including updates to ΔT_{Plio} and ΔF_{Plio} but excluding pattern effects ($\Delta\lambda$); (orange) fully updated SW20 including $\Delta\lambda$. **(b)** Posterior probability density functions (PDFs) after combining lines of evidence: (gray, white fill) SW20, (gray) SW20 with updated paleoclimate ΔT and ΔF but excluding $\Delta\lambda$, (orange) including $\Delta\lambda$ only for the Pliocene, (blue) $\Delta\lambda$ only for the Last Glacial Maximum (LGM) [3], and (orange, blue fill) Full Update including Pliocene and LGM $\Delta\lambda$. Panels **a–b** show effective climate sensitivity (S), as in SW20. **(c)** Projected global warming from the FaIR model [47], measured as mean anomaly over 2081–2100 relative to 1850–1900 mean, using climate sensitivity distributions from IPCC AR6 [16], SW20, and the Full Update in panel **b**. Line caps indicate 5th to 95th percentiles, dots indicate 66% *likely* range, box indicates 25th to 75th percentiles, and line indicates median.

tities (i.e., excluding $\Delta\lambda$), which increases ECS substantially. We then include $\Delta\lambda$ from only the Pliocene or LGM [3], and finally we combine our results for Pliocene and LGM $\Delta\lambda$ to provide a best estimate that fully accounts for paleoclimate pattern effects and their uncertainties. Once again, *global-mean* paleoclimate updates increase ECS, while the *spatial information* from pattern effects is more impactful and leads to much stronger overall constraints, particularly for the upper bound. The revised best estimate (median) for modern ECS becomes 2.8°C , with a 66% range of $2.4\text{--}3.4^{\circ}\text{C}$ (90% CI: $2.1\text{--}4.0^{\circ}\text{C}$) (Fig. 4b; Table S3). This range represents a major update to the upper bounds in SW20 [2] and the IPCC Sixth Assessment report (AR6) [16], while our lower bound confirms previous assessments. For comparison with SW20's robustness tests, we find a 66% robust range of $2.6\text{--}3.8^{\circ}\text{C}$ (90% CI: $2.3\text{--}4.6^{\circ}\text{C}$), which also represents a much stronger constraint compared to the 95th percentile of 5.7°C in SW20's robust range.

Importantly, our updates to modern ECS also reduce uncertainty in projections of 21st-century warming. Fig. 4c shows the 2081–2100 mean warming relative to 1850–1900 projected by the FaIR model [47], a climate emulator that produced projections for IPCC AR6, under SSP2-4.5 [16]. FaIR's large ensemble is calibrated to match the historical record through 2022 while sampling the full range of uncertainty in ECS [47]. We first revise the FaIR ensemble's ECS distribution to match SW20, which produces a minor change (Methods). We then use our fully updated ECS distribution with the FaIR model (Fig. 4b), which yields a median of 2.5°C and substantially reduces uncertainty in the upper bound of warming projections, with a 66% *likely* range for end-of-century warming of $2.1\text{--}2.9^{\circ}\text{C}$ (90% CI: $1.9\text{--}3.2^{\circ}\text{C}$).

Pliocene pattern effects arise from changes in ice sheets and vegetation that amplify SST warming in the extratropics, in turn leading to cloud feedbacks that further amplify global warming. Recent work on the Last Glacial Maximum also found that ice sheets amplify extratropical SST cooling, similarly leading to positive cloud feedbacks [3]. Because of these paleoclimate pattern effects from non-CO₂ forcings, the modern climate feedback from CO₂ alone is more stabilizing than the feedbacks associated with the Pliocene and LGM.

Neglecting pattern effects, and including updates only to *global means*, results in substantially higher estimates of climate sensitivity compared to SW20 [2] and IPCC AR6 [16]. We find that including *spatial information* leads to the opposite conclusion, such that paleoclimates now provide much stronger constraints on projected warming and the modern climate's sensitivity to CO₂. We note that our 21st-century projections assume ice sheets will not be lost this century, thus an important corollary to our results is that a major shift in the modern warming pattern, e.g., caused by loss of the West Antarctic Ice Sheet [23, 27, 45], could activate positive feedbacks in the modern climate similar to those that amplified global warming during the Pliocene.

316 Methods

317 AGCM Experiments

Following ref. [3], estimating paleoclimate $\Delta\lambda$ (Eq. 3) in AGCMs requires three simulations that differ only in their SST/SIC boundary conditions while all other forcings are constant at modern levels, similar to “amip-piForcing” experiments [12, 48].

The three categories of AGCM simulations are: **(a)** Preindustrial baseline, for which we use the Late Holocene (0–4 ka) [8]; **(b)** 2xCO₂, for which we use the multi-model mean of quasi-equilibrium 2xCO₂ simulations in LongRunMIP [31]; **(c)** Pliocene, for which we use the various reconstructions described in the main text (Fig. 1; Fig. S1–S3). In CAM4 and CAM5, we also test the 5th and 95th percentiles of the plioDA ensemble (Fig. S4); ensemble members are ranked by estimating λ_{Plio} with CAM4 Green's functions [39]. SST/SIC boundary conditions are prepared as described in ref. [3]. We use plioDA's SIC for ref. [6], as no SIC is provided by the latter; this approach is supported by similar ΔT_{Plio} in both reconstructions.

For each AGCM, we compute anomalies in simulations **(b)** and **(c)** relative to **(a)**. Simulations are 30 years, and we analyze means over the final 25 years for CAM4 (2° resolution), CAM5.3 (2°), CAM6.0 (2°) [49], and HadGEM3-GC3.1-LL (N96, 135 km) [50], or the final 30 of 31 years for GFDL-AM4.0 (C96, 100 km) [51]. Results are included in Tables S1–S2. As described in ref. [3], we test sensitivity of $\Delta\lambda$ to the 2xCO₂ pattern by computing an alternate $\Delta\lambda_{150\text{yr}}^{\text{Alt}}$, which uses the 150-year regression of abrupt CO₂-forcing simulations in the parent coupled models corresponding to each AGCM instead of our $\lambda_{2\text{xCO}_2}$. Each coupled model produces a distinct warming pattern over the 150-year period, thus $\Delta\lambda_{150\text{yr}}^{\text{Alt}}$ samples uncertainty in CO₂-warming patterns. This test confirms our finding of $\Delta\lambda < 0$ (Table S1–S2) and produces ECS constraints that agree with our main result within 0.1°C (Table S3). We decompose λ into component feedbacks (Planck, lapse rate, water vapor, surface albedo, shortwave cloud, and longwave cloud) using CAM5 radiative kernels [52], following ref. [38] (Fig. S5–S8).

Modern Climate Sensitivity from Pliocene and Combined Evidence

Modern climate sensitivity is the steady-state response of global-mean T to doubling preindustrial CO₂ concentrations, including only the feedbacks acting on an approximate 150-year timescale, i.e., assuming fixed ice sheets and vegetation. This metric, called “effective climate sensitivity” to distinguish it from true equilibrium, is termed S in SW20 [2] and hereafter. To infer S from Pliocene evidence, we build on SW20’s equation of Pliocene energy balance by including the updates described below (distribution percentiles provided in Table S3).

$$\Delta T_{\text{Plio}} = \frac{-\Delta F_{\text{CO}_2} (1 + f_{\text{CH}_4}) + \Delta F_{\text{NonGHG}}}{\frac{\lambda_{2\text{xCO}_2}}{1+\zeta} + \Delta\lambda} \quad (5)$$

(i) Our main update is incorporating Pliocene $\Delta\lambda$ as $\Delta\lambda \sim \mathcal{N}(\mu = -0.37, \sigma = 0.32)$ W m⁻² K⁻¹. We estimate μ and σ for $\Delta\lambda$ by combining the spread across AGCMs and reconstructions using the bootstrap approach in ref. [3], with plioDA’s best estimate as the reference value for differences in CAM4 and CAM5.

(ii) Pliocene forcing is updated based on the recent estimate of effective radiative forcing from non-GHG sources (ΔF_{NonGHG}), including ice sheets, vegetation, and land-sea distribution [23]. We assign $\Delta F_{\text{NonGHG}} \sim \mathcal{N}(1.7, 1.0)$ W m⁻² K⁻¹, which assumes a 1 σ uncertainty that approximately maintains the original SW20 uncertainty in total ΔF_{Plio} . For reference, total ΔF_{Plio} (numerator of Eq. 5) is 3.9±1.2 (1 σ) W m⁻², with $\Delta F_{\text{CO}_2} \approx 2.2$ W m⁻². We note there is substantial uncertainty in the components of ΔF_{Plio} , which merit further study [17, 19, 53–57].

363 (iii) ΔT_{Plio} is updated from $3.0 \pm 1.0^\circ\text{C}$ (1σ) in SW20 to plioDA's constraint of
 364 $\Delta T_{\text{Plio}} \sim \mathcal{N}(4.1, 0.6)^\circ\text{C}$ [5], which is supported by the estimate in ref. [6] of $3.9 \pm 1.1^\circ\text{C}$ (1σ).

365 From SW20 [2], the remaining parameters in Equation 5 are: CO₂ forcing of $\Delta F_{\text{CO}_2} =$
 366 $\Delta F_{2x\text{CO}_2} \times \ln(\frac{[\text{CO}_2]}{284\text{ppm}}) / \ln(2)$, where $[\text{CO}_2] \sim \mathcal{N}(375, 25)$ ppm and $\Delta F_{2x\text{CO}_2} \sim \mathcal{N}(4.0, 0.3) \text{ W m}^{-2}$;
 367 a scaling factor for methane and N₂O forcing, $1+f_{CH_4}$, with $f_{CH_4} \sim \mathcal{N}(0.4, 0.1)$; and
 368 a timescale transfer factor between quasi-equilibrium and the 150-year S timescale, $1+$
 369 ζ , to account for feedbacks becoming more positive at longer timescales, with $\zeta \sim \mathcal{N}(0.06, 0.2)$
 370 based on LongRunMIP [31]. Finally, modern climate sensitivity is $S = -\Delta F_{2x\text{CO}_2} / \lambda_{2x\text{CO}_2}$
 371 [2].

372 We also use an alternate version of the $\Delta\lambda$ in (i) estimated by comparing our
 373 paleoclimate AGCM simulations with feedbacks from 150-year regression of abrupt CO₂-
 374 forcing simulations in the parent coupled models of each AGCM. Each coupled model
 375 produces a distinct warming pattern, thereby sampling uncertainty in the pattern of warming
 376 from CO₂. With $\lambda_{150\text{yr}}^{\text{CO}_2}$ representing the regression feedback, we estimate Pliocene
 377 $\Delta\lambda_{150\text{yr}}^{\text{Alt}} = \lambda_{150\text{yr}}^{\text{CO}_2} - \lambda_{\text{Plio}}$, and we use the same bootstrap approach in (i) to find Pliocene
 378 $\Delta\lambda_{150\text{yr}}^{\text{Alt}} \sim \mathcal{N}(\mu = -0.44, \sigma = 0.40) \text{ W m}^{-2} \text{ K}^{-1}$. Because $\Delta\lambda_{150\text{yr}}^{\text{Alt}}$ represents a com-
 379 parison with the 150-year regression feedback rather than quasi-equilibrium simulations,
 380 the denominator of Equation 5 becomes $(\lambda_{2x\text{CO}_2} + \Delta\lambda_{150\text{yr}}^{\text{Alt}}) / (1 + \zeta)$ when using $\Delta\lambda_{150\text{yr}}^{\text{Alt}}$
 381 instead of our standard $\Delta\lambda$. Note that the percentiles of the final S distribution agree
 382 within 0.1°C when using $\Delta\lambda_{150\text{yr}}^{\text{Alt}}$ (Table S3).

383 There are advantages to our formulation of the Pliocene energy balance (Eq. 5) com-
 384 pared to SW20's Equation 23. First, the Pliocene is now consistent with the LGM, as
 385 ΔF_{NonGHG} is now added directly rather than estimated by multiplying ΔF_{CO_2} by a scale
 386 factor, $1+f_{ESS}$, representing Earth system sensitivity [1, 27]. Second, f_{ESS} conflates
 387 forcings and feedbacks, and estimating f_{ESS} requires free-running coupled simulations
 388 that have inaccurate warming patterns [23]. Instead of using f_{ESS} , our Equation 5 sep-
 389 arately includes *effective radiative forcing*, ΔF_{NonGHG} , from AGCM simulations with pa-
 390 leoenvironmental boundary conditions informed by proxies for ice extent, vegetation, and
 391 topography [23, 58], and *paleoclimate pattern effects*, from AGCM experiments with SST/SIC
 392 patterns constrained by data assimilation [3].

393 Climate sensitivity PDFs are summarized in Table S3. We calculate likelihoods and
 394 PDFs for S using SW20's Bayesian framework [2]. This framework quantitatively com-
 395 bines our findings with additional lines of evidence, and the methods can be continually
 396 developed in ongoing efforts [59, 60]. Our findings would have the same directional im-
 397 pact on other assessments of ECS and modern warming [16, 61].

398 In Fig. 4 and Table S3, we show S with and without updates (i), (ii), and (iii).
 399 For the LGM evidence in Fig. 4b, we include updated $\Delta T_{\text{LGM}} \sim \mathcal{N}(-6, 1)^\circ\text{C}$ and LGM
 400 $\Delta\lambda \sim \mathcal{N}(-0.37, 0.23) \text{ W m}^{-2} \text{ K}^{-1}$ [3]. We also use $\lambda_{150\text{yr}}^{\text{CO}_2}$ in Table S1 to estimate LGM
 401 $\Delta\lambda_{150\text{yr}}^{\text{Alt}} \sim \mathcal{N}(\mu = -0.42, \sigma = 0.34) \text{ W m}^{-2} \text{ K}^{-1}$. While SW20's framework generally
 402 assumes lines of evidence are independent, our estimates of Pliocene and LGM pattern
 403 effects are interrelated. We use the same AGCMs, and the reconstruction methods are
 404 partially overlapping. To account for the relationship between Pliocene and LGM $\Delta\lambda$
 405 estimates, we identify pairs of estimates that use similar reconstruction methods and the
 406 same AGCM (Table S4). From these pairs, we estimate the Pearson correlation (r) and
 407 covariance for $\Delta\lambda$ to be $r = 0.56$ and $\text{cov} = 0.0123 [\text{W m}^{-2} \text{ K}^{-1}]^2$. For $\Delta\lambda_{150\text{yr}}^{\text{Alt}}$, we

408 estimate $r = 0.87$ and $\text{cov} = 0.0562 [\text{W m}^{-2} \text{K}^{-1}]^2$. We account for the covariance
 409 by drawing correlated values for LGM and Pliocene $\Delta\lambda$ from bivariate normal distribu-
 410 tions. However, the S constraints are insensitive to the covariance, as our Full Update
 411 percentiles (Table S3) change by less than 0.1°C if we assume zero covariance.

412 We include results corresponding to SW20's robustness test, which assumes a uni-
 413 form prior on S from 0 to 20°C instead of the baseline prior of uniform λ from -10 to
 414 $10 \text{ W m}^{-2} \text{K}^{-1}$, in Table S3. The robustness test yields a median of 3.1°C and 66% range
 415 of $2.6 - 3.8^\circ\text{C}$ (90% CI: $2.3 - 4.6^\circ\text{C}$). As for our main result using the baseline prior,
 416 this represents a substantial narrowing of uncertainty compared to the robust ranges in
 417 SW20. For illustrative purposes, we also include posterior PDFs considering only the Pliocene
 418 evidence and assuming the uniform- S prior. The PDF from the Pliocene alone has a me-
 419 dian of 3.8°C and 66% range of $2.4 - 7.2^\circ\text{C}$ (90% CI: $1.9 - 12.9^\circ\text{C}$).

420 Projections of 21st-Century Warming

421 We analyze warming projections through 2100 under SSP2–4.5 [16] from the FaIR
 422 model v1.4.1, calibrated to match historical records as in IPCC AR6 but with updated
 423 constraints through 2022 [47]. From FaIR, we have a large ensemble of global-mean tem-
 424 peratures from 1850–2100, and each member has an associated ECS. For each ensem-
 425 ble member, we compute the mean warming over 2081–2100 relative to the 1850–1900
 426 mean. We then resample the ensemble with replacement to match the specified ECS dis-
 427 tributions from SW20 and from our updated paleoclimate-constrained ECS. This resam-
 428 pling produces revised distributions of projected warming that are associated with the
 429 specified ECS distributions (Fig. 4).

430 Data Availability

431 Model output and SST/SIC boundary conditions will be available on Zenodo upon
 432 publication. Pliocene reconstructions are available via refs. [5, 6]. Late Holocene recon-
 433 struction is available via ref. [8]. Effective radiative forcings for the Pliocene and mod-
 434 ern 2xCO_2 are available via ref. [23]. Results for LGM pattern effects are available via
 435 ref. [3]. LongRunMIP is available at longrunmip.org. CAM5 radiative kernels are avail-
 436 able via ref. [52]. Code for calculating ECS is available at doi.org/10.5281/zenodo.3945276 [2].

438 Author Contributions

439 VTC performed the analysis, designed the experiments, wrote the original draft,
 440 and ran the experiments in CAM4, CAM5, and CAM6. KCA and GJH supervised the
 441 study. KCA, GJH, CP, JET, NJB, and VTC obtained funding and computing resources.
 442 JET and MBO contributed plioDA and LGMR reconstructions. TA ran HadGEM3 and
 443 WD ran GFDL-AM4 experiments. MTD and RF contributed Pliocene-forcing simula-
 444 tions. All authors contributed to editing the manuscript. All authors declare no com-
 445 peting interests.

446 **Acknowledgments**

447 Funding sources: National Defense Science & Engineering Graduate (NDSEG) Fellow-
 448 ship, U.S. Department of Defense (VTC); National Science Foundation (NSF) award OCE-
 449 2002276 (VTC, KCA, GJH, MTD); National Oceanic and Atmospheric Administration
 450 MAPP Program award NA20OAR431039 (KCA, CP, MTD); Alfred P. Sloan Research
 451 Fellowship grant FG-2020-13568 (KCA); NSF award OCE-2002398 (JET, MBO); NSF
 452 award OCE-2002385 (CP); NSF award OCE-2002448 (NJB); NSF award AGS-1844380
 453 (NJB); Met Office Hadley Centre Climate Programme funded by DSIT (TA); NSF award
 454 OCE-2103055 (RF); NSF award AGS-2238875 (RF). VTC acknowledges computing sup-
 455 port from Derecho (doi:10.5065/qx9a-pg09) and Casper (<https://ncar.pub/casper>)
 456 provided by the NSF National Center for Atmospheric Research (NCAR), sponsored by
 457 NSF. The authors acknowledge NSF (No. 2238875) for funding a 2024 workshop on “Cli-
 458 mate evolution from early Eocene to mid-Pliocene,” which helped shape this work.

459 **References**

- [1] PALAEOSSENS Project Members, Making sense of palaeoclimate sensitivity. *Nature* **491**, 683–691 (2012).
- [2] SC Sherwood, et al., An Assessment of Earth’s Climate Sensitivity Using Multi-
ple Lines of Evidence. *Reviews of Geophysics* **58** (2020).
- [3] VT Cooper, et al., Last Glacial Maximum pattern effects reduce climate sensi-
tivity estimates. *Science Advances* **10**, 9461 (2024).
- [4] KD Burke, et al., Pliocene and Eocene provide best analogs for near-future
climates. *Proceedings of the National Academy of Sciences* **115**, 13288–13293
(2018).
- [5] JE Tierney, et al., Pliocene Warmth and Patterns of Climate Change Inferred
From Paleoclimate Data Assimilation. *AGU Advances* **6** (2025).
- [6] JD Annan, JC Hargreaves, T Mauritsen, E McClymont, SL Ho, Can we reli-
ably reconstruct the mid-Pliocene Warm Period with sparse data and uncertain
models? *Climate of the Past* **20**, 1989–1999 (2024).
- [7] JE Tierney, et al., Glacial cooling and climate sensitivity revisited. *Nature* **584**,
569–573 (2020).
- [8] MB Osman, et al., Globally resolved surface temperatures since the Last
Glacial Maximum. *Nature* **599**, 239–244 (2021).
- [9] AM Seltzer, et al., Widespread six degrees Celsius cooling on land during the
Last Glacial Maximum. *Nature* **593**, 228–232 (2021).
- [10] KC Armour, CM Bitz, GH Roe, Time-Varying Climate Sensitivity from Re-
gional Feedbacks. *Journal of Climate* **26**, 4518–4534 (2013).
- [11] T Andrews, JM Gregory, MJ Webb, The Dependence of Radiative Forcing and
Feedback on Evolving Patterns of Surface Temperature Change in Climate
Models. *Journal of Climate* **28**, 1630–1648 (2015).
- [12] JM Gregory, T Andrews, Variation in climate sensitivity and feedback param-
eters during the historical period. *Geophysical Research Letters* **43**, 3911–3920
(2016).
- [13] P Ceppi, JM Gregory, Relationship of tropospheric stability to climate sensitiv-
ity and Earth’s observed radiation budget. *Proceedings of the National Academy
of Sciences* **114**, 13126–13131 (2017).

- [491] [14] T Andrews, MJ Webb, The Dependence of Global Cloud and Lapse Rate Feed-
 492 backs on the Spatial Structure of Tropical Pacific Warming. *Journal of Climate*
 493 **31**, 641–654 (2018).
- [494] [15] E de la Vega, TB Chalk, PA Wilson, RP Bysani, GL Foster, Atmospheric CO₂
 495 during the Mid-Piacenzian Warm Period and the M2 glaciation. *Scientific*
 496 *Reports* **10**, 11002 (2020).
- [497] [16] P Forster, et al., 2021: The Earth’s energy budget, climate feedbacks, and cli-
 498 mate sensitivity in *Climate Change 2021: The Physical Science Basis. Contri-*
 499 *bution of Working Group I to the Sixth Assessment Report of the Intergovern-*
 500 *mental Panel on Climate Change*, eds. V Masson-Delmotte, et al. (Cambridge
 501 Univ. Press, Cambridge, UK and New York, NY), (2021).
- [502] [17] PO Hopcroft, et al., Polar amplification of Pliocene climate by elevated trace
 503 gas radiative forcing. *Proceedings of the National Academy of Sciences* **117**,
 504 23401–23407 (2020).
- [505] [18] U Salzmann, et al., Challenges in quantifying Pliocene terrestrial warming
 506 revealed by data–model discord. *Nature Climate Change* **3**, 969–974 (2013).
- [507] [19] H Dowsett, et al., The PRISM4 (mid-Piacenzian) paleoenvironmental recon-
 508 struction. *Climate of the Past* **12**, 1519–1538 (2016).
- [509] [20] DJ Lunt, et al., On the causes of mid-Pliocene warmth and polar amplification.
 510 *Earth and Planetary Science Letters* **321–322**, 128–138 (2012).
- [511] [21] JE Tierney, AM Haywood, R Feng, T Bhattacharya, BL Otto-Bliesner,
 512 Pliocene Warmth Consistent With Greenhouse Gas Forcing. *Geophysical*
 513 *Research Letters* **46**, 9136–9144 (2019).
- [514] [22] LE Burton, et al., On the climatic influence of CO₂ forcing in the Pliocene. *Cli-*
 515 *mate of the Past* **19**, 747–764 (2023).
- [516] [23] M Dvorak, et al., Mid-Pliocene climate forcing, sea-surface temperature pat-
 517 terns, and implications for modern-day climate sensitivity. *Journal of Climate*
 518 (*in press*). (2025).
- [519] [24] JE Weiffenbach, et al., Unraveling the mechanisms and implications of a
 520 stronger mid-Pliocene Atlantic Meridional Overturning Circulation (AMOC)
 521 in PlioMIP2. *Clim. Past* **19**, 61–85 (2023).
- [522] [25] R Feng, et al., Past terrestrial hydroclimate sensitivity controlled by Earth
 523 system feedbacks. *Nature Communications* **13**, 1306 (2022).
- [524] [26] S Menemenlis, JM Lora, M Lofverstrom, D Chandan, Influence of stationary
 525 waves on mid-Pliocene atmospheric rivers and hydroclimate. *Global and Plane-*
 526 *tary Change* **204**, 103557 (2021).
- [527] [27] DJ Lunt, et al., Earth system sensitivity inferred from Pliocene modelling and
 528 data. *Nature Geoscience* **3**, 60–64 (2010).
- [529] [28] GJ Hakim, et al., The last millennium climate reanalysis project: Framework
 530 and first results. *Journal of Geophysical Research: Atmospheres* **121**, 6745–6764
 531 (2016).
- [532] [29] R Caballero, M Huber, State-dependent climate sensitivity in past warm cli-
 533 mates and its implications for future climate projections. *Proceedings of the*
 534 *National Academy of Sciences* **110**, 14162–14167 (2013).
- [535] [30] I Eisenman, KC Armour, The radiative feedback continuum from Snowball
 536 Earth to an ice-free hothouse. *Nature Communications* **15**, 6582 (2024).

- [31] M Rugenstein, et al., LongRunMIP: Motivation and Design for a Large Collection of Millennial-Length AOGCM Simulations. *Bulletin of the American Meteorological Society* **100**, 2551–2570 (2019).
- [32] DE Amrhein, GJ Hakim, LA Parsons, Quantifying Structural Uncertainty in Paleoclimate Data Assimilation With an Application to the Last Millennium. *Geophysical Research Letters* **47** (2020).
- [33] AM Haywood, et al., The Pliocene Model Intercomparison Project Phase 2: large-scale climate features and climate sensitivity. *Climate of the Past* **16**, 2095–2123 (2020).
- [34] NJ Burls, AV Fedorov, What Controls the Mean East–West Sea Surface Temperature Gradient in the Equatorial Pacific: The Role of Cloud Albedo. *Journal of Climate* **27**, 2757–2778 (2014).
- [35] E Erfani, NJ Burls, The Strength of Low-Cloud Feedbacks and Tropical Climate: A CESM Sensitivity Study. *Journal of Climate* **32**, 2497–2516 (2019).
- [36] HL Ford, et al., Sustained mid-Pliocene warmth led to deep water formation in the North Pacific. *Nature Geoscience* **15**, 658–663 (2022).
- [37] EL McClymont, et al., Lessons from a high-CO₂ world: An ocean view from 3 million years ago. *Climate of the Past* **16**, 1599–1615 (2020).
- [38] BJ Soden, et al., Quantifying Climate Feedbacks Using Radiative Kernels. *Journal of Climate* **21**, 3504–3520 (2008).
- [39] Y Dong, C Proistosescu, KC Armour, DS Battisti, Attributing Historical and Future Evolution of Radiative Feedbacks to Regional Warming Patterns using a Green’s Function Approach: The Preeminence of the Western Pacific. *Journal of Climate* **32**, 5471–5491 (2019).
- [40] MW Wara, AC Ravelo, ML Delaney, Permanent El Nino-Like Conditions During the Pliocene Warm Period. *Science* **309**, 758–761 (2005).
- [41] AV Fedorov, et al., The Pliocene Paradox (Mechanisms for a Permanent El Nino). *Science* **312**, 1485–1489 (2006).
- [42] CL O’Brien, et al., High sea surface temperatures in tropical warm pools during the Pliocene. *Nature Geoscience* **7**, 606–611 (2014).
- [43] C Brierley, N Burls, C Ravelo, A Fedorov, Pliocene warmth and gradients. *Nature Geoscience* **8**, 419–420 (2015).
- [44] NJ Burls, AV Fedorov, Wetter subtropics in a warmer world: Contrasting past and future hydrological cycles. *Proceedings of the National Academy of Sciences* **114**, 12888–12893 (2017).
- [45] JE Weiffenbach, et al., Highly stratified mid-Pliocene Southern Ocean in PlioMIP2. *Climate of the Past* **20**, 1067–1086 (2024).
- [46] C Wang, et al., Diagnosing the Factors That Contribute to the Intermodel Spread of Climate Feedback in CMIP6. *Journal of Climate* **38**, 663–674 (2025).
- [47] C Smith, et al., fair-calibrate v1.4.1: calibration, constraining, and validation of the FaIR simple climate model for reliable future climate projections. *Geoscientific Model Development* **17**, 8569–8592 (2024).
- [48] T Andrews, Using an AGCM to Diagnose Historical Effective Radiative Forcing and Mechanisms of Recent Decadal Climate Change. *Journal of Climate* **27**, 1193–1209 (2014).

- 582 [49] G Danabasoglu, et al., The Community Earth System Model Version 2
583 (CESM2). *Journal of Advances in Modeling Earth Systems* **12** (2020).
- 584 [50] KD Williams, et al., The Met Office Global Coupled Model 3.0 and 3.1 (GC3.0
585 and GC3.1) Configurations. *Journal of Advances in Modeling Earth Systems*
586 **10**, 357–380 (2017).
- 587 [51] IM Held, et al., Structure and Performance of GFDL’s CM4.0 Climate Model.
588 *Journal of Advances in Modeling Earth Systems* **11**, 3691–3727 (2019).
- 589 [52] AG Pendergrass, A Conley, FM Witt, Surface and top-of-atmosphere radiative
590 feedback kernels for CESM-CAM5. *Earth Syst. Sci. Data* **10**, 317–324 (2018).
- 591 [53] A Haywood, et al., Pliocene Model Intercomparison Project Phase 3
592 (PlioMIP3) – Science plan and experimental design. *Global and Planetary*
593 *Change* **232**, 104316 (2024).
- 594 [54] GR Grant, et al., The amplitude and origin of sea-level variability during the
595 Pliocene epoch. *Nature* **574**, 237–241 (2019).
- 596 [55] N Sagoo, T Storelvmo, Testing the sensitivity of past climates to the indirect
597 effects of dust. *Geophysical Research Letters* **44**, 5807–5817 (2017).
- 598 [56] A Dutton, et al., Sea-level rise due to polar ice-sheet mass loss during past
599 warm periods. *Science* **349** (2015).
- 600 [57] N Unger, X Yue, Strong chemistry-climate feedbacks in the Pliocene. *Geophysical Research Letters* **41**, 527–533 (2014).
- 601 [58] J Zhu, CJ Poulsen, Last Glacial Maximum (LGM) climate forcing and ocean
602 dynamical feedback and their implications for estimating climate sensitivity.
603 *Climate of the Past* **17**, 253–267 (2021).
- 604 [59] K Marvel, M Webb, Towards robust community assessments of the Earth’s
605 climate sensitivity. *Earth System Dynamics* **16**, 317–332 (2025).
- 606 [60] SC Sherwood, CE Forest, Opinion: Can uncertainty in climate sensitivity be
607 narrowed further? *Atmospheric Chemistry and Physics* **24**, 2679–2686 (2024).
- 608 [61] D Kaufman, V Masson-Delmotte, Opinion: Distribute paleoscience information
609 across the next Intergovernmental Panel on Climate Change reports. *Climate of*
610 *the Past* **20**, 2587–2594 (2024).